ACS Chemical Neuroscience

Research Article

pubs.acs.org/chemneuro

Electroosmotic Push–Pull Perfusion: Description and Application to Qualitative Analysis of the Hydrolysis of Exogenous Galanin in Organotypic Hippocampal Slice Cultures

Amy E. Rupert,[†] Y. Ou,[†] M. Sandberg,[‡] and S. G. Weber*[,†]

[†]Department of Chemistry, University of Pittsburgh, Pittsburgh, Pennsylvania 15260, United States

[‡]Department of Medical Biochemistry and Cell Biology, Gothenburg University, Gothenburg, S 405 30 Sweden

Supporting Information

ABSTRACT: We demonstrate here a method that perfuses a small region of an organotypic hippocampal culture with a solution containing an enzyme substrate, a neuropeptide. Perfusate containing hydrolysis products is continually collected and subsequently analyzed for the products of the enzymatic degradation of the peptide substrate. The driving force for perfusion is an electric field. The fused silica capillaries used as "push" and "pull" or "source" and "collection" capillaries have a ζ-potential that is negative and greater in magnitude than the tissue's ζ-potential. Thus, depending on the magnitudes of particular dimensions, the electroosmotic flow in the capillaries augments the fluid velocity in the tissue. The flow rate is not directly measured; however, we determine it using a finite-element approach. We have determined the collection efficiency of the system using an all D-amino acid internal standard. The flow rates are low, in the nL/min range, and adjustable by controlling the current or voltage in the system. The collection efficiency of the D-amino acid peptide internal standard is variable, increasing with increased current and thus electroosmotic flow rate. The collection efficiency can be rationalized in the context of a Peclet number. Electroosmotic push–pull perfusion of the neuropeptide galanin (gal1–29) through the extracellular space of an organotypic hippocampal culture results in its hydrolysis by ectopeptidase reactions occurring in the extracellular space. The products of hydrolysis were identified by MALDI-MS. Experiments at two levels of current (8–12 μA and 19–40 μA) show that the probability of seeing hydrolysis products (apparently from aminopeptidases) is greater in the Cornu Ammonis area 3 (CA3) than in the Cornu Ammonis area 1 (CA1) in the higher current experiments. In the lower current experiments, shorter peptide products of aminopeptidases (gal13–29 to gal20–19) are seen with greater frequency in CA3 than in CA1 but there is no statistically significant difference for longer peptides (gal3–29 to gal12–29).

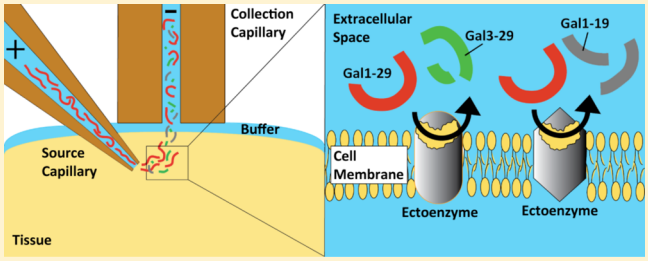

KEYWORDS: *Ectopeptidase, galanin, hippocampus, electroosmosis, neuropeptide, hydrolysis*

Galanin, a 29-amino acid neuropeptide (30 in humans), can reduce glutamate concentrations in the hippocampus after ischemia[1] and is protective against hippocampal cell death after exposure to exogenous glutamate or staurosparine.[2] This trophic effect is mediated by ligand binding of the GalR2 receptor.[3] The hippocampus is particularly vulnerable to ischemic cell death[4] and has a high density of galaninergic innervation[5,6] as well as a high density of glia expressing the GalR2 receptor,[3,7,8] suggesting that galaninergic pathways may be important in hippocampal function and survival after ischemic stress.

A neuropeptide's efficacy is ultimately determined by its effect on a target receptor. Factors that govern extrasynaptic (volume) transmission and activation of target receptors include the quantity released into the extracellular space, reuptake (if any), diffusion, and degradation in the extracellular space by ectopeptidases.[9] We focus on this latter case. The half-life of galanin has been studied in hypothalamus homogenates, spinal cord homogenates, and cerebrospinal fluid. Galanin-degrading enzymes were identified as belonging to the metalloprotease or aminopeptidase (which often themselves require metal for catalysis) class of enzymes.[10] While inactivation is typically thought of as the primary function of ectopeptidases,[11] some hydrolysis products may retain the ability to activate the galanin receptor.[10,12] When the first two residues, G1 and W2, are present, binding affinity to the GalR2 receptor is high.[13] Peptides without the N-terminal amino acids may also be active. Galanin fragments 12–29, 18–29, and 21–29 displace 40–55% of ^{125}I-galanin from its bound state on receptors (subtype unspecified) on the rat ventral hippocampus.[12] Fragment 17–29 also has a small binding affinity to hippocampal galanin receptors.[12]

Special Issue: Monitoring Molecules in Neuroscience

Received: March 28, 2013
Accepted: April 24, 2013
Published: April 24, 2013

The organotypic hippocampal slice culture (OHSC)[14,15] has been useful to the study of many aspects of brain function and disease, including but not limited to neurogenesis,[16,17] synaptic plasticity,[18,19] neurotoxicity,[15,20,21] stroke/ischemia,[5,22,23] and neuroprotection and repair.[24−26] The hippocampal formation is highly heterogeneous with several distinct neuronal populations with different functions, innervating and projecting to different areas of the brain.[27] Response to ischemic stress is different in different areas of the hippocampus: the Cornu Ammonis area 1 (CA1) is more vulnerable than the Cornu Ammonis area 3 (CA3) or dentate gyrus (DG) to models of oxidative stress and transient ischemia.[23,28] This difference in vulnerability extends to other models of injury and neuronal stress, including hypoglycemia and certain models of Alzheimer's disease.[29,30] The subgranular zone of the DG is likewise distinctive as it is one of the only areas of the brain undergoing neurogenesis,[31] which may reduce vulnerability to injury.[32] Developing a method to sample the extracellular space with enough spatial resolution to distinguish the neurochemistry in the various substructures within the hippocampus in a culture preparation with a total volume of about 1 μL would be highly advantageous for understanding how the hippocampus responds to injury.

There has been work on determining the products of enzymatic action on peptides in vivo.[33−36] In the cited work, the investigators used microdialysis. Peptide solutions were pumped into the probe and hydrolysis products were collected in the effluent. A few years ago, we introduced electroosmotic sampling, illustrating its use for studying enzymatic processes in tissue culture systems. Electroosmosis results when a current passes through a porous medium with a nonzero ζ-potential. The OHSC has a significant ζ-potential[37] and supports electroosmotic flow.[38] When using electroosmosis, low flow rates (nL/min) can be generated and controlled by changing the current and/or applied field. In our first electroosmotic sampling design, we took advantage of electroosmotic flow in living brain tissue to assess quantitatively the hydrolysis of exogenous leu-enkephalin by ectoenzymes in the extracellular space.[38,39] That work used a single capillary placed perpendicular to the tissue culture. The application of a field drew leu-enkephalin-containing buffered physiological electrolyte solution through the insert membrane and tissue. This single-capillary method has some advantages over the microdialysis method for tissue cultures because of relatively large size of the microdialysis probe, which must be inserted into the tissue. In addition, microdialysis relies on diffusion for transport outside of the probe, thus the time that the peptide is exposed to the extracellular space cannot be controlled. In addition, the extraction efficiency of higher molecular weight peptides can be rather low. In the single-capillary electroosmotic sampling experiment, the flow of fluid follows the current flow. The (positive) current flows from the tissue, converging on the capillary lumen. The spatial resolution is therefore limited. The method also wastes peptide, as less than a microliter of the 1.2 mL peptide-containing solution is used in the experiment.

We describe here an improved method that allows more control over the volume and path by which the peptide travels through extracellular space of the OHSC. The design is related conceptually to recent work on low flow rate push−pull perfusion, exploiting the method's superior spatial resolution, low flow rates (10−50 nL/min), and minimal damage.[40,41] Electroosmotic push−pull perfusion (EOPPP), however, is driven by electroosmosis rather than pressure. There is no membrane associated with the EOPPP probe; thus, this method is compatible with large MW substrates. It is further compatible with both acute and cultured tissue preparations.

We calculated the flow rate by finite-element analysis of the Brinkman equation under various experimental conditions of applied voltage/current, capillary dimensions, and placement. We also examined how porosity affects sampling efficiency by sampling from a hydrogel that has a similar ζ-potential to that of an OHSC.[42] We then use EOPPP to investigate the hydrolysis of galanin. Samples were analyzed by MALDI-TOF/TOF to identify hydrolytic products of enzymatic activity in the CA1 and CA3 regions of the hippocampus.

RESULTS AND DISCUSSION

Electroosmotic push−pull perfusion (EOPPP) is illustrated in Figure 1. A source capillary with a tapered tip (inside diameter (i.d.) at the tip: 15−30 μm) was inserted into the OHSC. A collection capillary (i.d. 50−150 μm) was nearby in contact with the surface of the tissue through a thin layer of electrolyte solution. Applying a voltage across the capillaries drove fluid from the source capillary through the tissue and into the collection capillary. In contrast to our previous work described above, the (positive) current flows from a small, approximately 20 μm diameter opening in the "push" pipet through tissue to the thin layer of electrolyte solution and into the collection capillary. The volume perfused is considerably smaller than in our earlier approach. Thus, the spatial resolution is, in principle, improved.

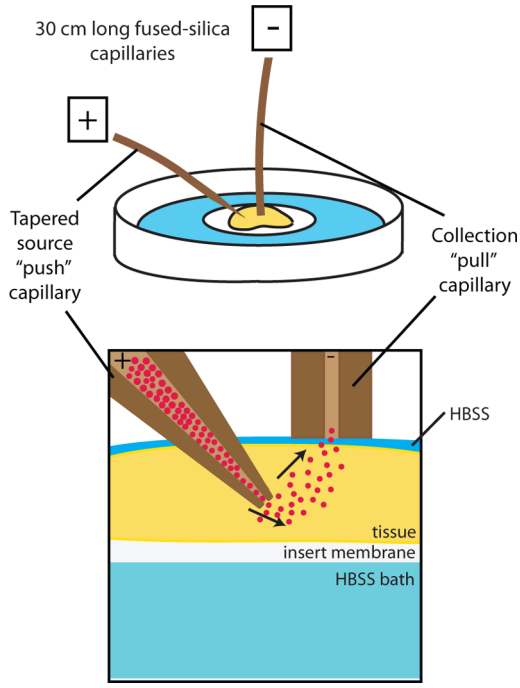

Figure 1. Electroosmotic push−pull perfusion. The OHSC sits on the insert membrane over an HBSS bath. The tapered tip of the source capillary is inserted into the tissue while the collection capillary is in contact with a thin layer of HBSS fluid on top of the tissue. A potential difference is applied to a pair of electrodes at the proximal end of each capillary causing current flow and electroosmotic flow, passing from the tapered source capillary to the collection capillary.

Relationship between Flow Rate and Electrical Parameters. We begin with the relationship between the

dx.doi.org/10.1021/cn400082d | ACS Chem. Neurosci. 2013, 4, 838−848

volume-averaged fluid electroosmotic velocity and the electric field in the tissue. We consider the tissue to be a porous medium analogous to a packed bed of nonporous particles. The porous medium (tissue) contains electrolyte in the interstitial (extracellular) volume. The nonporous particles (cells) are nonconducting under the conditions used, i.e., we are applying fields below the threshold for electroporation.[43] Following Hlushkou et al.[44] and using the thin double-layer approximation, we can write eq 1.

$$v_{eo,vol} = -\frac{\epsilon_w \zeta}{\eta}\vec{E}\left(\frac{\sigma_{tiss}}{\sigma_{el}}\right) \quad (1)$$

The volume-averaged electroosmotic fluid velocity, $v_{eo,vol}$, is inversely proportional to the fluid viscosity (η), and it is proportional to the electric field, $\vec{E}$, the permittivity of the electrolyte, ϵ_w, the tissue ζ-potential, ζ, and a ratio of the conductivity, σ_{tiss}, of the tissue to the conductivity of the electrolyte in the absence of the nonconducting, nonporous particles (σ_{el}). The volume-averaged velocity, or superficial velocity, is the volume flow rate of fluid through a given total (i.e., porous and nonporous) area. The utility of this velocity is that it is conserved, for example, in a serial arrangement of porous and nonporous sections of a conduit of constant cross section because the flow rate is conserved. It is also the velocity that is specified in Darcy's Law for pressure-induced flow of an incompressible fluid through a porous medium, eq 2.

$$v_{p,vol} = \frac{\kappa}{\eta}\frac{\Delta P}{L} \quad (2)$$

In models of porous media, the ratio ($\sigma_{tiss}/\sigma_{el}$) is related to the porosity, ϕ (electrolyte-filled volume as a fraction of total volume when the particles are nonporous), and tortuosity, λ.[45] The latter is often estimated, especially in the neurochemistry context, as the square root of the ratio of a molecular diffusion coefficient in the electrolyte alone to the diffusion coefficient in the tissue.[46−48] We note that this definition results in a tortuosity that depends on what molecule is diffusing. In the pure fluid flow context, the definition must relate to the diffusion of solvent molecules, the so-called geometric tortuosity. Using this model, we define eq 3.

$$\left(\frac{\sigma_{tiss}}{\sigma_{el}}\right) = \frac{\phi}{\lambda^2} \quad (3)$$

Also, using this model, we can define the average linear velocity as shown in eq 4

$$v_{eo,al} = \frac{v_{eo,vol}}{\phi} \quad (4)$$

It is convenient to relate velocities and flow rates to current rather than the electric field. We know that the externally applied electric field and the average current density in a porous medium are related as in eq 5

$$J = \vec{E}\sigma_{tiss} \quad (5)$$

Here, the conductivity is that of the tissue (porous medium) and the current density (J) is the apparent current density: that observed in the laboratory from knowledge of the current flowing through the porous medium and the total cross sectional area, A. Further, recognizing that the electroosmotic mobility, μ_{eo}, is defined as in eq 6, and the volume flow rate, U_{eo}, as in eq 7, we can write the relationship between current (i) and volume flow rate of fluid ($v_{eo,vol}$) as eq 8.

$$\mu_{eo} = -\frac{\epsilon_w \zeta}{\eta} \quad (6)$$

$$U_{eo} = A v_{eo,vol} \quad (7)$$

$$U_{eo} = \mu_{eo}\frac{i}{\sigma_{el}} \quad (8)$$

We note that eq 8 applies to open conduits such as fused silica capillaries as well as porous media. The measured conductivity of HBSS is 1.43 S m^{-1}. In a capillary that has walls with a −50 mV ζ-potential,[49] the electroosmotic mobility is 4.0×10^{-8} m^2 V^{-1} s^{-1}. In the tissue with an average ζ-potential of −21.3 mV,[49] the electroosmotic mobility is 1.70×10^{-8} m^2 V^{-1} s^{-1}. The ratio of flow rate to current (U_{eo}/i) is 1.18×10^{-8} m^3 A^{-1} s^{-1} in the tissue and 2.78×10^{-8} m^3 A^{-1} s^{-1} in the capillary. In more practical units, these flow rates are 0.71 and 1.67 nL min^{-1} μA^{-1}.

In the case of EOPPP, Figure 1, electroosmosis occurs at different velocities in the capillaries and the tissue. The conservation of mass dictates that the mass flow rate in an incompressible medium must be conserved. The mismatch in ζ-potentials creates a pressure that in turn creates a pressure-induced flow. The total flow rate is thus conserved. This problem is difficult to solve in the general case because the resultant flow rate depends on details such as tissue hydraulic permeability, exact dimensions in the pulled capillary, and distances traveled in each portion of the overall flow path. Thus, we turned to finite- element simulations of EOPPP.

Finite-Element Calculation of the Flow Rate. Using COMSOL Multiphysics (v4.3a), we first created a simple cylindrical model to test the congruence of the simulations to eq 8. Flow in a 100 μm i.d. open capillary with a wall ζ-potential of −50 mV was modeled. Flow in tissue was modeled as a cylindrical object with a defined ζ-potential (−21.3 mV), porosity, tortuosity, and hydraulic permeability. The flow rates were calculated by integrating the volume-average velocity (m s^{-1}) over a cross-sectional surface between the two ends of the cylindrical model. In both cases, the finite element modeling resulted in ratios of flow rate to current that differ by less than 1% of the values calculated by eq 8. With confidence in our treatment of the problem by finite element methods, we simulated the three-dimensional EOPPP setup in COMSOL. A sketch of the model is shown in Supporting Information Figure SI-1. Tables SI-1 and SI-2 list all relevant constants and boundary conditions for the model.

We demonstrated that the flow rate was linearly related to either current or applied voltage over a range of conditions (data not shown). Thus, we will discuss the flow rates as ratios to current. The collection flow rate for EOPPP is 2.52×10^{-8} m^3 A^{-1} s^{-1} (or 1.51 nL min^{-1} μA^{-1}; 200 μm source barrel i.d., 20 μm source tip i.d. inserted 60 μm into the tissue, and 100 μm collection capillary), a value between that calculated for the capillary only and that calculated for the porous tissue model only. This flow rate was lower than we calculated for the capillary alone (1.67 nL min^{-1} μA^{-1}) because of the presence of the tissue. The fluid flow rate in the collection capillary was equal to the fluid flow rate in the source capillary (1.06 nL min^{-1} μA^{-1}) plus the fluid flow rate through the bottom of the tissue (0.44 nL min^{-1} μA^{-1}). This suggests that some sample dilution occurs because of this drawing of fluid from the HBSS

buffer underneath. The flow rate in the tissue through a surface parallel to the long axis of the collection capillary placed between the opening of the source capillary and to the left of the collection capillary lumen was 1.37×10^{-8} m^3 A^{-1} s^{-1}, or 0.82 nL min^{-1} μA^{-1}. This flow rate was higher than what we calculated for the tissue alone (0.71 nL min^{-1} μA^{-1}) due to the presence of the capillaries. Because of the geometry of the system, this flow rate depends on exactly where the measurement surface is placed.

To understand how various linear dimensions of the sampling geometry (e.g., source lumen size, insertion depth, capillary-to-tissue distance, collection capillary size) influence flow rate, we modeled commonly used sets of conditions and changed the size of each dimension one at a time. Our calculations showed that independent changes in source tip i.d., the distance that the source tip is place below the surface (DBS) and the thickness of the electrolyte layer between the capillary and the tissue (CTD) did not have a significant effect on the flow-rate-to-current or flow-rate-to-field ratios (data not shown). Changing the collection i.d., however, did cause a change in these two ratios. Figure 2 reports this effect. As about

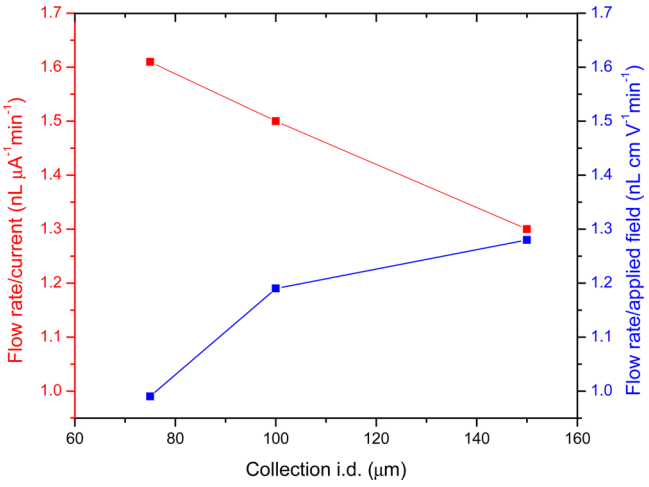

Figure 2. Effect of collection i.d. on flow rate in the collection capillary. The small but apparent effect of the collection i.d. on the flow-rate-to-current ratio is caused by the ζ-potential mismatch of the capillary walls and the tissue. Because the capillary ζ-potential magnitude is greater than the tissue's, the mismatch creates a small positive pressure at the source-tip-and-tissue junction and a small negative pressure in the droplet, which induces a pressure-induced flow. The observed flow-rate-to-current ratio is lower than that of the capillary alone (1.67 nL min^{-1} μA^{-1}) and greater than that of the tissue alone (0.71 nL min^{-1} μA^{-1}). The magnitude of the pressure-induced flow is greater the greater the flow resistance of the capillaries. The smaller i.d. collection capillary with its higher flow resistance supports a greater pressure gradient at the capillary-tissue junction. As we increase the collection i.d., the pressure decreases and the flow rate decreases.

99.9% of the electrical resistance in the circuit is the electrolyte in the two 30 cm long capillaries, the applied field was calculated by summing the total voltage drop across the two capillaries divided by the total length (60 cm). The companion paper to this article shows that the voltage drop in the tissue is minimal compared to that in the two capillaries.[50]

The effect of the collection i.d. on the flow-rate-to-field ratio can be explained by Ohm's law in conjunction with the ζ-potential mismatch. As the i.d. of the collection capillary increases from 75 to 150 μm, the overall electrical resistance decreases, current increases as does flow rate. At the same time, the flow resistance of the capillary decreases, so the increase in flow is less than expected from the change in electrical resistance alone.

Estimation of the Recovery of the Internal Standard. Figure 3 shows a section of a typical chromatogram with GGFL, galanin, and $^{D}Y^{D}AG^{D}F^{D}L$ (IS) peaks identified.

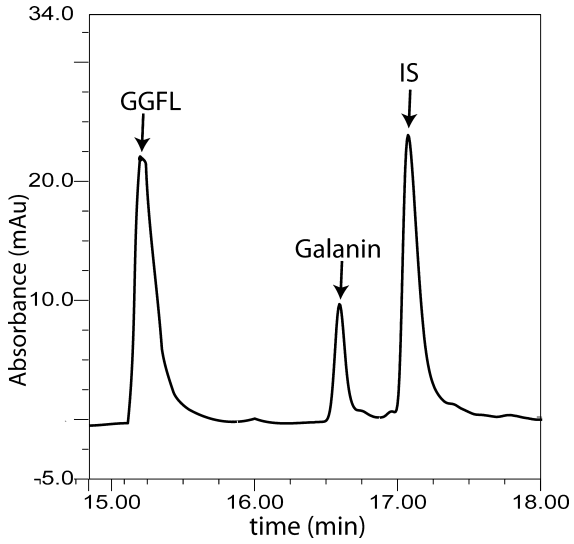

Figure 3. Section of a chromatogram of galanin with IS and GGFL. GGFL was used as an external standard for determining the volume of sample injected. TR3 is not identified, as it is not seen under the conditions used.

The peptide GGFL was included in all samples as an external standard to account for variability in HPLC injection volume. The GGFL calibration curve was linear over an injected concentration range of $9 - 40$ μM. Each sample and standard injected had the same concentration of GGFL allowing us to assess the consistency of the injected volumes over time. While moles of GGFL injected as assessed by HPLC peak area, and thus the injection volume, was quite consistent (the relative standard deviation in a given day was in the range of 1−3%), all peak areas were corrected for this variation. An all D-amino acid peptide, $^{D}Y^{D}AG^{D}F^{D}L$, was used as an internal standard (IS). D-Amino acid peptides are resistant to enzymatic hydrolysis. Though not pertinent for estimating flow rate, galanin was also part of the sample and eluted between GGFL and IS. The concentration of IS in the sample was determined from its peak area in the HPLC in comparison to IS calibration curves. This concentration was then multiplied by the total sample volume (12.36 μL) to find the number of moles of internal standard collected in the capillary ($moles_{IS}$), as shown in eq 9.

$$moles_{IS} = [IS]_{sample} \times V_{sample} \quad (9)$$

The number of moles collected is related to the number of moles injected into the tissue and the fraction of that number of moles that is collected. This fraction depended on many parameters. Here, we estimated the fractional recovery by calculating the volume of IS solution in the source capillary that would contain the number of moles of IS that was found in the collection capillary. This volume (V_{IS}) was calculated by dividing the number of moles of internal standard collected by

the initial concentration in the source capillary ($[IS]_{source}$) as shown in eq 10.

$$V_{IS} = \frac{moles_{IS}}{[IS]_{source}} \quad (10)$$

An equivalent flow rate, U_{eq}, is the ratio of V_{IS} to the sampling time, eq 11.

$$U_{eq} = \frac{V_{IS}}{t_s} \quad (11)$$

The volume of collected internal standard (V_{IS}) in both tissue and gel is plotted against experimental current in Figure 4.

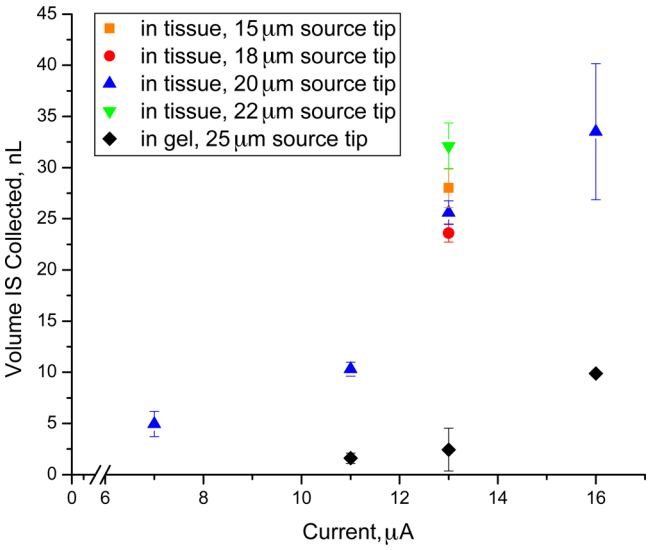

Figure 4. Volume of internal standard collected versus current. For all points, the source barrel i.d. was 200 μm tip inserted 60 μm into the tissue or gel. The collection i.d. was 100 μm and was raised 25 μm from the tissue surface. The colored data points represent sampling in tissue, n = 216. The black points represent sampling in gel, n = 19.

From Figure 4, we see that the volume collected in the gel under nearly identical sampling conditions is much less than that in the tissue − about 10 times smaller. In EOPPP, when fluid moves between the capillaries, there is a zone of high IS concentration directed toward collection by convective flow (electroosmosis). At the same time, the concentration gradient favors IS diffusion away from the current path. The effect of these influences became evident when comparing TR3 fluorescence during perfusion of tissue and gels. When sampling in the tissue, the TR3 fluorescence was detected as it left the source and accumulated around the collection capillary. Accumulation in the surrounding tissue was apparent. However, when sampling in the gel, only the TR3 that was captured in the collection capillary was visible. There was no visible accumulation in the gel. The interplay of these convective and diffusional forces can be understood in the context of a Peclet number, defined in eq 12

$$Pe = va/D \quad (12)$$

v is the deterministic velocity of a solute, a is a characteristic length which is constant in this case, and D is the diffusion coefficient. Both v and D are influenced by the porosity and tortuosity of a porous medium. The electric field for a given current is higher when the porosity is smaller. Thus the electroosmotic velocity is higher in the tissue than in the gel as the gel porosity is near unity.[42] Second, the tortuosity impedes both diffusion and fluid flow, though, there is a molecular weight dependence on reported observed tortuosity in porous media.[48,51] In the gel, the tortuosity as determined by using the solute TR3 is near unity[42] so there is little effect of tortuosity in the gel. In the tissue, the effect of the tortuosity decreases the diffusion coefficient more than the average linear velocity, promoting effective collection. Thus, Pe in the tissue is significantly higher than in the gel.

Table 1 tabulates the volume of IS collected under a particular sampling geometry (200 μm source capillary, 20 μm tip, 60 μm insertion depth, 100 μm collection capillary i.d., 25 μm CTD) and compares this to the volume of IS collected under similar conditions in the gel as well as our calculations of how much IS is being injected into the tissue/gel. Table 1 also shows the calculated collection efficiencies. These increase as the current increases. As the convective velocity increases as current increases, but the characteristic dimension, a, and diffusion coefficient, D, are independent of current, the increase in current increases Pe. The increase in Pe leads directly to an increase in collection efficiency.

The low flow rates indicate that discretely collected samples will be small. In our experiments, we calculate that we typically collected on the order of 0.1−0.2 μL of IS that is ultimately diluted to about 12 μL prior to analysis (see the Methods section for details). During HPLC analysis, a 1 μL injection volume was preconcentrated on a 75 μm i.d. reversed phase column. Thus, each analysis used approximately 8% of what was initially a 0.1−0.2 μL sample (i.e., a volume on the order of 12 nL of extracellular fluid is analyzed). If the concentration of the species of interest is not high enough to provide a quantifiable or detectable number of moles of analyte, there are several ways to improve the overall sensitivity, aside from the obvious solution of a better detector. Samples can be collected at higher voltages (better collection efficiency) for longer times, fluid management can be improved to avoid dilution,[41] smaller HPLC columns can be used, and a larger volume of sample can be injected.

We anticipated that the spatial resolution of this approach to sampling would be governed by the current flow path. In qualitative support of this idea, we have recorded images of the fluorescence from a 3000 MW Texas Red-labeled dextran (TR3), which is initially in the source pipet. Figure SI-4

Table 1. Collection Efficiency of Injected Solute into Tissue and Gel

current (μA)	field (V cm^{-1})	collected volume IS, in tissue (nL)	collected volume IS, in gel (nL)	volume IS injected into tissue (nL)	volume IS injected into gel (nL)	collection efficiency in tissue	collection efficiency in gel
7	3.33	4.9 ± 1.2		74.2	68.7	6.7%	
11	5	10.3 ± 0.7	1.6 ± 0.5	106	98	9.7%	1.6%
13	6.66	23.6 ± 0.9	5.2 ± 0.6	137	128	17%	4.1%
16	8.33	33.5 ± 6.7	9.9	169	157	20%	6.3%

dx.doi.org/10.1021/cn400082d | ACS Chem. Neurosci. 2013, 4, 838−848

demonstrates that the fluorescence is confined to the area under the collection capillary.

Galanin Hydrolysis. In earlier work,[36] we established that peptide hydrolysis occurred in the tissue, but not in the collection capillary. We thus infer that our results are not a result of cytoplasmic peptidases, released from damaged cells, being pulled into the collection capillary. This is consistent with our findings on the extent of damage caused by the technique.[50]

In designing the experiment, we chose the substrate (galanin) concentration (158 μm) based on several factors. First, we wanted the concentration of the hydrolysis products in the collected sample to be at a detectable level after losses in the sampling process itself (collection efficiency < 100%), dilution in the collection capillary, and dilution in the water/TFA solution prior to injection into the HPLC. However, we also wanted the concentration to be low enough so as to adequately reflect the activity of peptidases that would be acting against biologically relevant concentrations of galanin. Unfortunately, there are no publications on K_m values for galanin, so we must be guided by studies of other peptides. In our previous studies, we found the K_m of enkephalin-degrading ectopeptidases to be 1.2 mM.[38] Other studies report K_m values for corticotrophin releasing factor-degrading ectopeptidases ranging from 42 to 165 μM,[52] for membrane-bound aminopeptidases acting on amino acid napthylamides values of 20−1120 μM,[53,54] and 45 μM for enkephalin-degrading aminopeptidase M.[55] The chosen concentration is a compromise that yields detectable quantities of hydrolysis products for biologically relevant processes.

Table SI-3 tallies a list of galanin fragments identified according to the criteria set forth in the Methods section below. To investigate if there were any differences in hydrolysis in different regions of the hippocampus, we determined the frequency with which we saw a particular fragment in a particular hippocampal region. To this end, we grouped MS data into six categories in each of the two regions: CA1 and CA3. The six categories result from two levels of current created during sampling: "low" (8−12 μA) and "high" (19−40 μA) in combination with three sets of observed peptides: those products containing the amine terminus (gal1-*X*), those longer products containing the carboxy terminus (*X*-29, *X* = 3−12), and those shorter products containing the carboxy terminus (*X*-29, *X* = 13−20). Frequencies low and high current conditions for the CA1 and CA3 are shown in Figure 5. These sampling conditions create little damage.[50]

The intact galanin peptide, gal1−29, was found in all samples. All hydrolysis products collected retained either the N-terminus or the C-terminus. There is only one complementary pair of peptides, gal1−19 and gal20−29, that could be the result of a single enzyme cleavage event. Of course, the complementary peptide to the longer products found, for example, gal3−29 and gal1−27, would not be seen in the MALDI spectrum because of their low molecular mass. Nonetheless, the results are consistent with many of the products being the result of several enzymes acting in sequence. The peptides with intact N-termini may be a result of the action of carboxypeptidases. One plausible candidate is enkephalin convertase (carboxypeptidase E, 3.4.17.10), which is a membrane bound peptidase expressed in the hippocampal DG and CA3 pyramidal layers. This peptidase preferentially cleaves off arginine and lysine residues and may explain gal1−19 and gal1−27.[56−59] The plurality of products with an intact C-terminus indicates aminopeptidase activity. Several products

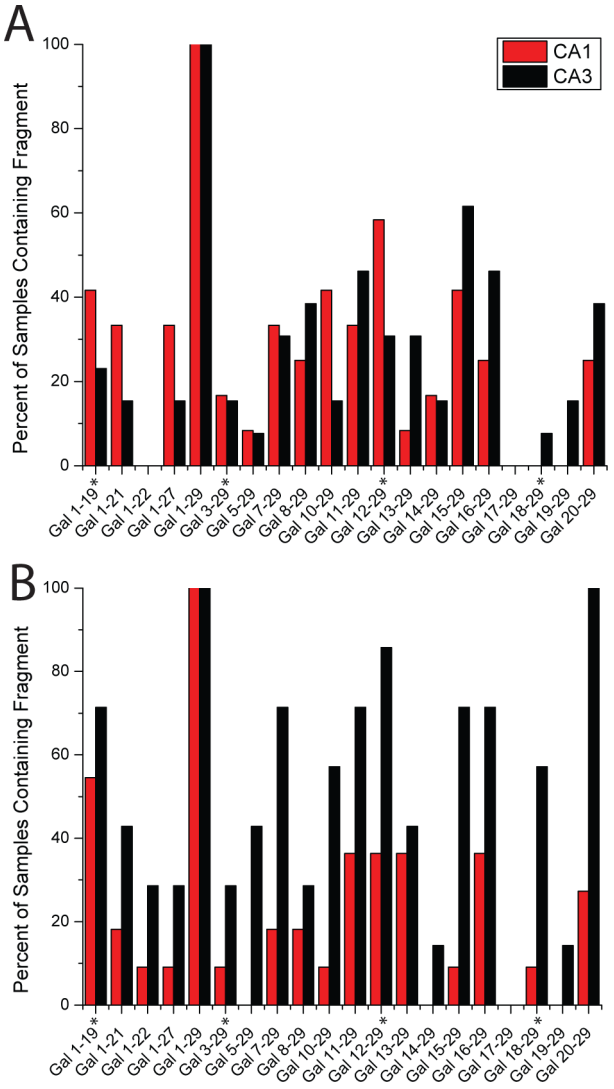

Figure 5. Comparison of frequency of fragments found in CA3 versus CA1 samples. (A) Sampling was performed with 8−12 μA of current (n = 12 for CA1, n = 13 for CA3). (B) Sampling with 19−40 μA. All samples contained the intact 1−29 galanin peptide (n = 11 for CA1, n = 7 for CA3). Asterisks (*) indicate fragments that have binding affinity to galanin receptors (discussed in the text).

differ in length by two amino acids (gal3−29, 5−29, 7−29, as well as 8−29 and 10−29) suggesting the action of a dipeptidyl peptidase. Dipeptidyl peptidase III (3.4.14.4) fits the activity profile as it is classified a dipeptidyl aminopeptidase and has activity in the rat brain.[60] Samples contained several products (gal3−29, 12−29, and 18−29, 1−19) that display binding affinity to the galanin receptor[12] (* in Figure 5). Other products contain the residues important for strong binding (G1 and W2)[13] although the binding affinities of gal1−21, 1−22, and 1−27 have not been reported.

To assess the differences in the CA1 and CA3, we tested whether the observed frequencies in the six categories described above demonstrated statistically significant differences by analysis of two-way tables. There were differences in frequencies of observing products with amine termini intact but with low statistical significance based on a chi squared statistic (low current, p = 0.089, total number of observations, N = 100, CA1 frequency greater than CA3; high current, p = 0.071, N = 72, CA3 frequency greater than CA1). In both low

dx.doi.org/10.1021/cn400082d | ACS Chem. Neurosci. 2013, 4, 838−848

and high current conditions, the probability of finding short peptides with intact carboxy termini was higher in the CA3 (low current, $p = 0.032$, $N = 200$; high current, $p < 0.001$, $N = 144$). In high current, but not low current conditions, the probability of finding long peptides with intact carboxy termini was higher in the CA3 (low current, $p = 0.503$, $N = 175$; high current, $p < 0.001$, $N = 126$).

Damage. The flow rates in electroosmotic push−pull perfusion are less than those routinely used in low-flow push−pull perfusion[40,61−64] and thus also likely do not cause any damage arising from the physical force of moving fluid on delicate cells. The companion paper to this article[50] outlines conditions for minimizing damage associated with electroosmotic push−pull perfusion. There is no physical damage from insertion of source capillary into tissue; however, the electric field in the tissue can have damaging effects. We chose the conditions to test here based on conditions tested in previous and to coincide with concurrent studies of damage associated with EOPPP.[50,65] Applied currents of 13 μA in 100 μm i.d. or smaller collection capillaries induce little damage, and as seen here, create flow rates that are below the 10 nL min^{-1} threshold but also are fast enough to collect a detectable quantity of source analyte.

CONCLUSIONS

Most determinations of peptidase activity, and enzyme activity in general, are performed in homogenates or membrane preparations. The application of microdialysis to the problem was a leap forward because it measured peptidase activity in intact tissue,[33,35] although one must be aware of the damage that microdialysis causes in the region being sampled.[66] In addition, the membrane may place limitations on the size of peptides that can be delivered. In certain applications, such as small animals such as mice and in tissue cultures, the size of the probe is also an issue. The method presented here is the first method that allows the study of enzymatic reactions by the introduction of natural substrate into and through the extracellular space in a controlled, spatially resolved manner. The spatial resolution of EOPPP is improved over our previous electroosmotic sampling design as electroosmotic and thus sample collection flow follows the current path, which is essentially limited to the region between the two capillaries rather than between a capillary and the solution below the tissue.

The simulations of EOPPP revealed the interesting and not entirely unexpected fact that the process induces pressure flow. The electroosmotic flow in the capillary augments the electroosmotic flow in the tissue because the ζ-potential on the capillary walls exceeds that of the tissue. The majority of the fluid collected in the collection capillary comes from the source capillary, however a fraction comes from the bath below the tissue. There is a disadvantage to this because of the difficulty in knowing what the actual flow rate will be when setting up an experiment. However, in the absence of pressure flow, it would still be difficult to know exactly what the flow rate in the tissue is. An internal standard for collection efficiency will always be required. At the same time, a potential problem that is seen in microfluidic work, that of the walls of the capillary being altered by the sample leading to changes in the electroosmotic mobility, is not likely to be significant here. Depending on conditions, the volume of fluid collected is only a fraction of the collection capillary's volume and the capillary is only used once. Thus wall effects are not expected to be dominant. On the other hand, the presence of pressure flow assists in minimizing the problem of electrophoretic bias in sampling.

The numerical modeling will allow us to investigate other designs or capillary orientations to create desired flow rates, spatial resolutions, collection efficiencies, and sensitivity to rate processes in the tissue. With these simulations, we will likely be able to reduce the number of animals/tissues we use investigating different sampling parameters; rather we can model first, predict, and verify with only a few animals/samples.

The extracellular metabolism of galanin has not been studied in hippocampal preparations, let alone in a living, biochemically functional hippocampal culture. Galanin may be an important component in the cellular mechanisms following ischemic stress, particularly with regards to promoting neuronal survival. It is well-known that ischemic stress is less well accommodated in the CA1 region in comparison to the CA3.[23,29] This work shows that the role of galanin in each area may also be different. This work sets the stage for and hints at the importance for a comprehensive quantitative analysis of the metabolism of galanin in the hippocampus.

METHODS

Solutions and Reagents. The culture medium was 50% opti-MEM, 25% horse serum, 25% Hank's balanced salt solution with phenol red (all from Gibco by Life Technologies, Carlsbad, CA), supplemented with 1% D-(+)-glucose (Sigma-Aldrich, St. Louis, MO), and filtered through a Nalgene filter (0.1 μm pore size, Fisher Scientific, Waltham, MA). The dissection solution was a serum-free version of the culture medium, substituting opti-MEM solution for the horse serum. Hank's balanced buffer solution (HBSS, Gibco by Life Technologies) was used during sampling, for rinsing of tissues, and for culture imaging. A 3 kDa Texas Red-dextran conjugate (TR3, Molecular Probes by Life Technologies) solution was prepared by dissolving it in HBSS. TR3 solutions were filtered through a 0.45 μm PTFE syringe filter and frozen until use. The D-amino acid peptide, $^{D}Y^{D}AG^{D}F^{D}L$, was prepared by the Peptide Synthesis Core at the University of Pittsburgh (Pittsburgh, PA) for use as an internal standard (IS). Solutions of the IS were prepared by dissolving peptide in HBSS. Galanin (rat, 1−29, Abbiotec, San Diego, CA) stock solution was prepared by adding 1 mL of HBSS to 1 mg solid galanin peptide. Both galanin and internal standard peptide solutions were frozen at −20°C until use. Aqueous solutions of 0.1% triflouroacetic acid (TFA, Sigma-Aldrich) were prepared by diluting it in deionized water (Millipore Synthesis A10) and filtering through a 0.45 μm PTFE syringe filter. GGFL peptide (Abcam, Cambridge, MA) was diluted in 0.1% TFA. A solution of 0.1% TFA in acetonitrile (ACN) was prepared by diluting stock TFA in ACN (Sigma-Aldrich), and filtering through a 0.45 μm PTFE syringe filter. Solutions of 50:50 v/v H_2O:ACN + 0.1% TFA were prepared by mixing the aqueous 0.1% TFA and ACN 0.1% TFA solutions. The MALDI matrix, α-cyano-4-hydroxycinnamic acid (CHCA, Sigma-Aldrich) was prepared by dissolving 10 mg of CHCA in 50:50 H_2O/ACN + 0.1% TFA acid and filtering through a 0.45 μm PTFE syringe filter. The MALDI-TOF/TOF instrument was calibrated using the mass standard kit for calibration of ABSciex TOF/TOF instruments (ABSciex, Foster City, CA).

Surgical and Culturing Procedure. Dissection and culturing techniques are identical to those previously used.[50] Briefly, the hippocampi of 7-day-old Sprague−Dawley rat pups were dissected and chopped along the septotemporal axis at a thickness of 350 μm. To plate, 2−3 slices were placed onto each porous (0.4 μm) modified PTFE insert membrane surface (Millipore, Bedford, MA), and cultured in a 6-well plate (Sarstedt, Newton, NC) over 1.2 mL of serum-containing medium. The OHSCs were incubated at 36.5 °C in 5% CO_2 and 95% air for 5−8 days before use. The medium was exchanged every 2−3 days during incubation. Prior to use, each OHSC was inspected by under bright field illumination (Olympus IX-71,

Melville, NY) for structural integrity and proper overall appearance and morphology prior to sampling. We discarded those in which any part of the hippocampal formation was unrecognizable or in which abnormal growth is observed.

Sampling: General Procedure. Before sampling can begin, the source and collection capillaries must be prepared, mounted, filled, and positioned. Both capillaries were made of fused silica (Polymicro Technologies, L.L.C., Phoenix, AZ). The collection capillary was cut to 30 cm with a Shortix capillary cutter (Scientific Instrument Services, Ringoes, NJ) with diamond blade to ensure a clean, straight cut to the end. The source capillary was prepared by pulling capillaries of 150−250 μm i.d. fused silica capillary to a bee-stinger-type tip using a capillary puller (Model P-2000, Sutter Instruments, Inc., Novato, CA). A razor blade was used to trim off the bee-stinger tip to create the desired tip diameter (15−25 μm). This process was monitored by visualization under bright field illumination with the IX-71 inverted microscope with a 4×, 0.16 NA objective (microscope and objective from Olympus, Melville, NY). Capillaries were positioned with electronic micromanipulators (model MP-285, Sutter Instruments, Inc.) on the IX-71 microscope stage. The source capillary was mounted at a 45° angle from the microscope stage while the collection capillary was perpendicular to the microscope stage. The proximal ends of each capillary were submerged in individual dishes filled with HBSS.

The collection capillary was filled with HBSS by a syringe at the proximal end of the capillary. To prevent clogging, the source capillary was backfilled by applying a vacuum to the proximal (untapered) end while the distal tapered tip is submerged in filtered fill solution (the preparation is described later).

A clean plastic Petri dish was held securely in place over the objective lens and filled with 1.2 mL HBSS. The dish could hold an insert membrane containing OHSCs or a ∼2 cm × 2 cm square of hydrogel (25% w/w acrylic acid, prepared as previously described[42]). The insert membrane with tissues was on top of the HBSS while the gel sits in the HBSS. The positions of each capillary were carefully monitored and controlled by the shadows the capillaries cast over the tissue or gel under bright field illumination. Figure SI-2 shows the capillary placement process. The source capillary tip were inserted into the tissue or gel at a desired insertion depth and the collection capillary positioned above the tissue or gel, in contact with HBSS solution, at a desired distance (capillary-to-tissue distance). The distance between the capillaries can be calculated using geometry according to the diagram in Figure SI-3. Platinum electrodes attached each HBSS-filled dish at each of the proximal ends of the capillaries to a high-voltage source (model PS350, Stanford Research Systems, Sunnyvale, CA).

Sampling was performed for one of two goals: to estimate the flow rate and to investigate the metabolism of galanin peptide while it is exposed to the extracellular space during sampling. In each experiment type, sampling conditions were slightly different.

Sampling of an Exogenous Solute. The source capillary fill solution was prepared by mixing 25% freshly thawed TR3, 25% IS solutions, and 50% galanin solution, creating a delivery solution which was 0.25−0.75 mM TR3, 2.73 mM $^{D}Y^{D}AG^{D}F^{D}L$, and 158.0 μM galanin. Sampling was performed using a 200 μm i.d. source capillary pulled to a tip of 15−25 μm inserted 60 μm into the tissue. The collection capillary was 100 μm raised 25 μm above the surface and 200−500 V (7−16 μA) were applied. In experiments using OHSCs, 4−6 tissues were removed from the incubator approximately 10−15 min before sampling commenced. Tissues remained over culture medium solution in 6-well plates. One tissue was sampled at a time and both tissues on an insert membrane were sampled before being placed back in the 6-well plate. In gels, a small piece of gel was put in a shallow bath of HBSS to keep the gel from drying. The gel was sampled multiple times, but each time in a new location, at least 2 mm away from a previously sampled spot. After 10 min of sampling, the contents of the collection capillary were pushed by an air-filled syringe into a vial containing 10 μL of 0.1% TFA/9.5 μM GGFL. Samples were injected (1 μL) into an HPLC (Ultimate 3000 Nano LC system, ThermoFisher, Waltham, MA) and separated on a trap column (75 μm × 2 cm, C18, 3 μm, 100 Å) inline with an analytical column (75 μm × 15 cm, C18, 2 μm, 100 Å) using gradient elution at a flow rate of 300 nL min^{-1}. The gradient started at 20% ACN and increased to 48% ACN in 9.75 min, returned back to 20% ACN in 1 min and re-equilibrated there for 6 min before the next injection. To prepare IS calibration standards, 10 μL of the source capillary fill solution was diluted to 1.00 mL in 0.1% TFA. This solution was then further diluted with 0.1% TFA and equal volumes of GGFL solution to make standards ranging from 2 to 10 μM IS each of which was also 6.65 μM in GGFL.

To ensure fluid flow between capillaries, TR3 fluorescence was imaged using the 4× 0.16 NA objective and U-MGIW2 filter set (Olympus). SimplePCI image acquisition software (Hamamatsu, Sewickley, PA) captured time-lapsed fluorescent images of TR3 moving from source to collection capillary. An example of this is shown in Figure SI-4.

Sampling to Investigate Galanin Metabolism. The fill solution was prepared with equal parts stock TR3 and stock galanin solutions. The source capillary was a 200 μm i.d. fused silica capillary with a tip tapered to 15−35 μm and inserted 40 or 60 μm below the tissue surface. The collection capillary was either 75 or 100 μm i.d. and was positioned 25 μm above the tissue surface. The CA3 and CA1 were target areas for sampling. Sampling was performed for 5 or 10 min by applying a voltage ranging from 200 to 400 V, inducing a current ranging from 6 to 10 μA. TR3 fluorescence was imaged identically as before.

After sampling, the contents of the collection capillary were pushed into a 10 μL aqueous solution of 0.1% TFA by an air-filled syringe. Each sample was desalted and concentrated using a μ-C18 ZipTip pipet tip (Millipore Corporation, Billerica, MA). ZipTips were first equilibrated with 20 μL 0.1% TFA in ACN then 20 μL 0.1% TFA in water. The sample was fully aspirated and dispensed 15−20 times. The ZipTip was then rinsed twice with 10 μL 0.1% TFA in water. The sample components retained on the ZipTip were eluted onto an Opti-TOF 384 Well Insert MALDI plate (Applied Biosystems by Life Technologies) with 0.8 μL of a 50:50 v/v mixture of water and ACN with 0.1% TFA. Each ZipTip was used only once. After the spot was dry, 0.4 μL 5 mg/mL CHCA was added to the top and allowed to dry. Spots were analyzed on a 4800 Plus MALDI TOF/TOF Mass Spectrometer (Applied Biosystems by Life Technologies) after verification of proper calibration through a mass standard mixture spotted on the plate.

MALDI spectra were viewed using the Data Explorer program (Applied Biosystems). Peak lists were compiled by including only those peaks with signal-to-noise ratio greater than 20. The list was input into the "findpept" program on Expasy (www.expasy.com) using galanin, GWTLN SAGYL LGPHA IDNHR SFSDK HGLT-NH_2, as the parent peptide and a mass tolerance of ±1.0 Da. The resultant matches to possible galanin fragments were subjected to a subsequent tandem mass spectral (MS/MS) analysis. Expected b and y ion peaks for the suspected fragment were found using the fragment ion calculator from the Institute for Systems Biology (http://db.systemsbiology.net:8080/proteomicsToolkit/index.html). The suspect galanin fragment sequence (including the amidation of the C-terminus if the C-terminus was part of the fragment) was entered into the database and the experimental spectrum was compared to the generated list of b and y ions for the suspect fragment. It was very clear if the spectrum matched the list or not. The b ion peak corresponding to the break between ^{17}D and ^{18}K, if these residues were present in the hydrolysis product, was the strongest peak. The first and last few b and y fragment ions are often are missing from MS/MS spectra. Thus spectra that contained 70% of the listed peaks were considered a positive match. Those that matched fewer than 70% were considered a negative match or inconclusive. A MS/MS spectrum of a previously identified hydrolysis product was obtained periodically to verify that a particular peak was still identified correctly.

Finite Element Method (FEM) Calculations. We used COMSOL Multiphysics to simulate the current path ("Electric Currents" module) and fluid flow ("Free and Porous Media Flow" module) for our EOPPP system. A 3D model with shortened capillaries and tissue was created with simple geometric shapes. The

tissue was treated as a homogeneous porous material with a defined porosity, tortuosity, hydraulic permeability, conductivity, and effective charge density. The "Electric Currents" module solved the Laplace equation for the voltage (V). All other electrical quantities, such as electric field, were derived from this. The "Free and Porous Media Flow" module solved the Brinkman equation for pressure and volume-averaged velocity. To determine the flow rate ($m^3\ s^{-1}$), we integrate the volume-averaged (i.e., superficial) velocity ($m\ s^{-1}$) over a cross-sectional surface (m^2) in the collection capillary.

■ ASSOCIATED CONTENT

Supporting Information

COMSOL model parameters; a table of galanin hydrolysis products, peptides, found and confirmed by CID fragmentation patterns; bright field images of the capillary positioning procedure; geometry of capillary placement; time-lapse fluorescence images of sampling. This material is available free of charge via the Internet at http://pubs.acs.org.

■ AUTHOR INFORMATION

Corresponding Author

*E-mail: sweber@pitt.edu.

Author Contributions

A.E.R. and S.G.W. designed the experiments, and all experiments were carried out by A.E.R. Y.O. did the numerical simulations. A.E.R., S.G.W., and Y.O. wrote the manuscript. M.S. participated in experimental design as well as providing guidance on galanin and related neurochemistry.

Funding

We acknowledge funding from the NIH through grant R01 GM044842 and an Arts & Sciences Fellowship from the Kenneth P. Dietrich School of Arts and Sciences to Y.O.

Notes

The authors declare no competing financial interest.

■ ACKNOWLEDGMENTS

We thank Emily Sun (Merck & Co.) for assistance in determining the appropriate statistical measures used to determine whether or not the frequencies of hydrolysis products are different in CA1 and CA3. We also thank Jonathan Cui for preparing the poly(acrylamide-co-acrylic acid) gels.

■ REFERENCES

(1) Zini, S., Roisin, M., Armengaud, C., and Ben-Ari, Y. (1993) Effect of potassium channel modulators on the release of glutamate induced by ischemic-like conditions in rat hippocampal slices. *Neurosci. Lett. 153*, 202−205.

(2) Elliott-Hunt, C., Marsh, B., Bacon, A., Pope, R., Vanderplank, P., and Wynick, D. (2004) Galanin acts as a neuroprotective factor to the hippocampus. *Proc. Natl. Acad. Sci. U.S.A. 101*, 5105−5110.

(3) Elliott-Hunt, C., Pope, R., Vanderplank, P., and Wynick, D. (2007) Activation of the galanin receptor 2 (GalR2) protects the hippocampus from neuronal damag. *J. Neurochem. 100*, 780−789.

(4) Lipton, P. (1999) Ischemic cell death in brain neurons. *Physiol. Rev. 79*, 1431−1568.

(5) Shen, P.-J., Yuan, C.-G., Ma, J., Chen, S., Yao, M., Turnley, A., and Gundlach, A. (2005) Galanin in neuro(glio)genesis: expression of galanin and receptors by progenitor cells in vivo and in vitro and effects of galanin on neurosphere proliferation. *Neuropeptides. 39*, 201−205.

(6) Melander, T., Hoekfelt, T., Roekaeus, A., Cuello, A., Oertel, W., Verhofstad, A., and Goldstein, M. (1986) Coexistence of galanin-like immunoreactivity with catecholamines, 5-hydroxytryptamine, GABA and neuropeptides in the rat CNS. *J. Neurosci. 6*, 3640−3654.

(7) Skofitsch, G., and Jacobowitz, D. (1985) Immunohistochemical mapping of galanin-like neurons in the rat central nervous system. *Peptides 6*, 509−546.

(8) Abbosh, C., Lawkowski, A., Zaben, M., and Gray, W. (2011) GalR2/3 mediates proliferative and trophic effects of galanin on postnatal hippocampal precursors. *J. Neurochem. 117*, 426−436.

(9) Bunnett, N. W. (1987) The role of neuropeptides in regulating airway function. Postsecretory metabolism of peptides. *Am. Rev. Respir. Dis. 136*, S27−S34.

(10) Land, T., Langel, U., and Bartfai, T. (1991) Hypothalamic degradation of galanin(1−29) and galanin(1−16): identification and characterization of the peptidolytic products. *Brain Res. 558*, 245−250.

(11) Hallberg, M., and Nyberg, F. (2003) Neuropeptide conversion to bioactive fragments - an important pathway in neuromodulation. *Curr. Protein Pept. Sci. 4*, 31−44.

(12) Fisone, G., Langel, U., Carlquist, M., Bergman, T., Consolo, S., Hoekfelt, T., Unden, A., Andell, S., and Bartfai, T. (1989) Galanin receptor and its ligands in the rat hippocampus. *Eur. J. Biochem. 181*, 269−276.

(13) Lang, R., Gundlach, A., and Kofler, B. (2007) The galanin peptide family: receptor pharmacology, pleiotropic biological actions, and implications in health and disease. *Pharmacol. Ther. 115*, 177−207.

(14) Stoppini, L., Buchs, P., and Muller, D. (1991) A simple method for organotypic cultures of nervous tissue. *J. Neurosci. Methods 37*, 173−182.

(15) Noraberg, J. (2004) Organotypic brain slice cultures: An efficient and reliable method for neurotoxicological screening and mechanistic studies. *ATLA, Altern. Lab. Anim. 32*, 329−337.

(16) Lindroos, M. M., Soini, S. L., Kukko-Lukjanov, T. K., Korpi, E. R., Lovinger, D., and Holopainen, I. E. (2005) Maturation of cultured hippocampal slices results in increased excitability in granule cells. *Int. J. Dev. Neurosci. 23*, 65−73.

(17) Poulsen, F., Blaabjerg, M., Montero, M., and Zimmer, J. (2005) Glutamate receptor antagonists and growth factors modulate dentate granule cell neurogenesis in organotypic, rat hippocampal slice cultures. *Brain Res. 1051*, 35−49.

(18) Holopainen, I. (2005) Organotypic hippocampal slice cultures: A model system to study basic cellular and molecular mechanisms of neuronal cell death, neuroprotection, and synaptic plasticity. *Neurochem. Res. 30*, 1521−1528.

(19) Lushnikova, I., Skibo, G., Muller, D., and Nikonenko, I. (2011) Excitatory synaptic activity is associated with a rapid structural plasticity of inhibitory synapses on hippocampal CA1 pyramidal cells. *Neuropharmacology 60*, 757−764.

(20) Won, R., Lee, K. H.., and Lee, B. H. (2011) Coenzyme Q10 protects neurons against neurotoxicity in hippocampal slice culture. *NeuroReport. 22*, 721−726.

(21) Takahashi, M., Liou, S.-Y., and Kunihara, M. (1995) Ca2+- and Cl–dependent, NMDA receptor-mediated neuronal death induced by depolarization in rat hippocampal organotypic cultures. *Brain Res. 675*, 249−256.

(22) Ziemka-Nalecz, M., Stanaszek, L., and Zalewska, T. (2013) Oxygen-glucose deprivation promotes gliogenesis and microglia activation in organotypic hippocampal slice culture: Involvement of metalloproteinases. *Acta Neurobiol. Exp. (Wars) 73*, 130−142.

(23) Vornov, J., Park, J., and Thomas, A. (1998) Regional vulnerability to endogenous and exogenous oxidative stress in organotypic hippocampal culture. *Exp. Neurol. 149*, 109−122.

(24) Simao, F., Zamin Laurenqq, L., Frozza, R., Nassif, M., Horn Ana, P., and Salbego Christianne, G. (2009) Protective profile of oxcarbazepine against oxygen-glucose deprivation in organotypic hippocampal slice culture could involve PI3K cell signaling pathway. *Neurol. Res. 31*, 1044−1048.

(25) Holopainen, I., Kukko-Lukjanov, T., and Lopez-Picon, F. (2005) Neuroprotection against kainic acid excitotoxicity by specific glutamate receptor antagonists in cultured organotypic hippocampal slices. *Trends Neurochem. Res.*, 145−164.

(26) Nakagami, Y., Saito, H., and Matsuki, N. (1997) Basic fibroblast growth factor and brain-derived neurotrophic factor promote survival

and neuronal circuit formation in organotypic hippocampal culture. *Jpn. J. Pharmacol. 75*, 319−326.
(27) Andersen, L.; Morris, R.; Amaral, D.; Bliss, T.; O'Keefe, J. *The Hippocampus Book*; Oxford University Press: New York, 2007.
(28) Butler, T., Self, R., Smith, K., Sharrett-Field, L., Berry, J., Littleton, J., Pauly, J., Mulholland, P., and Prendergast, M. (2010) Selective vulnerability of hippocampal cornu ammonis 1 pyramidal cells to excitotoxic insult is associated with the expression of polyamine-sensitive N-methyl–asparate-type glutamate receptors. *Neuroscience 165*, 525−534.
(29) Tasker, R. C., Coyle, J. T., and Vornov, J. J. (1992) The regional vulnerability to hypoglycemia-induced neurotoxicity in organotypic hippocampal culture: protection by early tetrodotoxin or delayed MK-801. *J. Neurosci. 12*, 4298−4308.
(30) Wang, X., Michaelis, M. L., and Michaelis, E. K. (2010) Functional genomics of brain aging and Alzheimer's disease: focus on selective neuronal vulnerability. *Curr. Genomics 11*, 618−633.
(31) Sawada, M., and Sawamoto, K. (2013) Mechanisms of neurogenesis in the normal and injured adult brain. *Keio J. Med. 62*, 13−28.
(32) Liu, J., Solway, K., Messing, R. O., and Sharp, F. R. (1998) Increased neurogenesis in the dentate gyrus after transient global ischemia in gerbils. *J. Neurosci. 18*, 7768−77678.
(33) Andren, P. E., and Caprioli, R. M. (1995) In vivo metabolism of substance P in rat striatum utilizing microdialysis/liquid chromatography/micro-electrospray mass spectrometry. *J. Mass Spectrom. 30*, 817−824.
(34) Eriksson, U., Andren, P. E., Caprioli, R. M., and Nyberg, F. (1996) Reversed-phase high-performance liquid chromatography combined with tandem mass spectrometry in studies of a substance P-converting enzyme from human cerebrospinal fluid. *J. Chromatogr., A 743*, 213−220.
(35) Nydahl, K. S., Pierson, J., Nyberg, F., Caprioli, R. M., and Andren, P. E. (2003) In vivo processing of LVV-hemorphin-7 in rat brain and blood utilizing microdialysis combined with electrospray mass spectrometry. *Rapid Commun. Mass Spectrom. 17*, 838−844.
(36) Sanderson, K., Andren, P. E., Caprioli, R. M., and Nyberg, F. (1996) In vitro metabolism of LVV-hemorphin-7 in human plasma studied by reversed-phase high-performance liquid chromatography and micro-electrospray mass spectrometry. *J. Chromatogr., A 743*, 207−212.
(37) Guy, Y., Faraji, A. H., Gavigan, C. A., Strein, T. G., and Weber, S. G. (2012) Iontophoresis from a micropipet into a porous medium depends on the zeta-potential of the medium. *Anal. Chem. 84*, 2179−2187.
(38) Xu, H., Guy, Y., Hamsher, A., Shi, G., Sandberg, M., and Weber, S. (2010) Electroosmotic sampling. Application to determination of ectopeptidase activity in organotypic hippocampal slice cultures. *Anal. Chem. 82*, 6377−6383.
(39) Hamsher, A. E. (2010) Development of electroosmotic sampling for the identification and quantification of neuropeptides and their metabolites in the extracellular space of the hippocampus. In *Monitoring Molecules in Neuroscience 2010* (Westerink B., Clinkers, R., Smolders I., Sarre S., and Michotte Y., Ed.), Vrije Universiteit Brussel: Brussels, Belgium and Fonds Wetenschappelijk Onderzoek: Vlaanderen.
(40) Kottegoda, S., Shaik, I., and Shippy Scott, A. (2002) Demonstration of low flow push-pull perfusion. *J. Neurosci. Methods 121*, 93−101.
(41) Slaney, T. R., Nie, J., Hershey, N. D., Thwar, P. K., Linderman, J., Burns, M. A., and Kennedy, R. T. (2011) Push-pull perfusion sampling with segmented flow for high temporal and spatial resolution in vivo chemical monitoring. *Anal. Chem. 83*, 5207−5213.
(42) Faraji, A., Cui, J., Guy, Y., Li, L., Gavigan, C., Strein, T., and Weber, S. (2011) Synthesis and characterization of a hydrogel with controllable electroosmosis: a potential brain tissue surrogate for electrokinetic transport. *Langmuir 27*, 13635−13642.
(43) Nolkrantz, K., Farre, C., Brederlau, A., Karlsson, R., Brennan, C., Eriksson, P., Weber, S., Sandberg, M., and Orwar, O. (2001) Electroporation of single cells and tissues with an electrolyte-filled capillary. *Anal. Chem. 73*, 4469−4477.
(44) Hlushkou, D., Seidel-Morgenstern, A., and Tallarek,, U. (2005) Numerical analysis of electroosmotic flow in dense regular and random arrays of impermeable, nonconducting spheres. *Langmuir 21*, 6097−6112.
(45) Scales, N., and Tait, R. N. (2006) Modeling electroosmotic and pressure-driven flows in porous microfluidic devices: Zeta potential and porosity changes near the channel walls. *J. Chem. Phys. 125*, 094714.
(46) Shen, L., and Chen, Z. (2007) Critical review of the impact of tortuosity on diffusion. *Chem. Eng. Sci. 62*, 3748−3755.
(47) Nicholson, C. (2001) Diffusion and related transport mechanisms in brain tissue. *Rep. Prog. Phys. 64*, 815−844.
(48) Hrabe, J., Hrabetova, S., and Segeth, K. (2004) A model of effective diffusion and tortuosity in the extracellular space of the brain. *Biophys. J. 87*, 1606−1617.
(49) Guy, Y., Sandberg, M., and Weber, S. (2008) Determination of ζ-potential in rat organotypic hippocampal cultures. *Biophys. J. 94*, 4561−4569.
(50) Rupert, A. E., Ou, Y., Sandberg, M., and Weber, S. G. (2013) Assessment of tissue viability following electroosmotic push-pull perfusion from organotypic hippocampal slice cultures. *ACS Chem. Neurosci.* DOI: 10.1021/cn4000814.
(51) Sykova, E., and Vargova, L. (2008) Extrasynaptic transmission and the diffusion parameters of the extracellular space. *Neurochem. Int. 52*, 5−13.
(52) Ritchie, J. C., Davis, T. P., and Nemeroff, C. B. (2003) Action of three ectopeptidases on corticotropin-releasing factor: metabolism and functional aspects. *Neuropsychopharmacology 28*, 22−33.
(53) Wachsmuth, E. D., and Donner, P. (1976) Conclusions about aminopeptidase in tissue sections from studies of amino acid naphthylamide hydrolysis. *Histochemistry 47*, 271−283.
(54) Krishnamoorthy, M., and Achary, A. (2013) Exploration of Sitagliptin as a potential inhibitor for the M1 Alanine aminopeptidase enzyme in Plasmodium falciparum using computational docking. *Bioinformation 9*, 293−298.
(55) Hersh, L. B., Aboukhair, N., and Watson, S. (1987) Immunohistochemical localization of aminopeptidase M in rat brain and periphery: relationship of enzyme localization and enkephalin metabolism. *Peptides 8*, 523−532.
(56) Fricker, L. D. (1988) Carboxypeptidase E. *Annu. Rev. Physiol. 50*, 309−321.
(57) Supattapone, S., Fricker, L. D., and Snyder, S. H. (1984) Purification and characterization of a membrane-bound enkephalin-forming carboxypeptidase, "enkephalin convertase". *J. Neurochem. 42*, 1017−1023.
(58) MacCumber, M. W., Snyder, S. H., and Ross, C. A. (1990) Carboxypeptidase E (enkephalin convertase): mRNA distribution in rat brain by in situ hybridization. *J. Neurosci. 10*, 2850−2860.
(59) Lynch, D. R., Strittmatter, S. M., Venable, J. C., and Snyder, S. H. (1986) Enkephalin convertase: localization to specific neuronal pathways. *J. Neurosci. 6*, 1662−1675.
(60) Prajapati, S. C., and Chauhan, S. S. (2011) Dipeptidyl peptidase III: a multifaceted oligopeptide N-end cutter. *FEBS J. 278*, 3256−3276.
(61) Kottegoda, S., Pulido, J., Thongkhao-on, K., and Shippy, S. (2007) Demonstration and use of nanoliter sampling of in vivo rat vitreous and vitreoretinal interface. *Mol. Vision 13*, 2073−2082.
(62) Piyankarage, S. C., Featherstone, D. E., and Shippy, S. A. (2012) Nanoliter hemolymph sampling and analysis of individual adult Drosophila melanogaster. *Anal. Chem. 84*, 4460−4466.
(63) Pritchett, J., Pulido, J., and Shippy, S. (2008) Measurement of region-specific nitrate levels of the posterior chamber of the rat eye using low-flow push-pull perfusion. *Anal. Chem. 80*, 5342−5349.
(64) Patterson, E. E., 2nd, Pritchett, J. S., and Shippy, S. A. (2009) High temporal resolution coupling of low-flow push-pull perfusion to capillary electrophoresis for ascorbate analysis at the rat vitreoretinal interface. *Analyst 134*, 401−406.

(65) Hamsher, A., Xu, H., Guy, Y., Sandberg, M., and Weber, S. (2010) Minimizing tissue damage in electroosmotic sampling. *Anal. Chem. 82*, 6370−6376.
(66) Jaquins-Gerstl, A., Shu, Z., Zhang, J., Liu, Y., Weber, S. G., and Michael, A. C. (2011) Effect of dexamethasone on gliosis, ischemia, and dopamine extraction during microdialysis sampling in brain tissue. *Anal. Chem. 83*, 7662−7667.